ESC European Society of Cardiology

Europace (2020) **22**, 1119–1131
doi:10.1093/europace/euaa093

BASIC SCIENCE

Dysferlin links excitation–contraction coupling to structure and maintenance of the cardiac transverse–axial tubule system

Julia Hofhuis [1,2†], Kristina Bersch[1†], Stefan Wagner[3], Cristina Molina[2,4‡], Funsho E. Fakuade[2,4], Lavanya M. Iyer[2,4¶], Katrin Streckfuss-Bömeke[2,5], Karl Toischer[2,5], Laura C. Zelarayán[2,4], Niels Voigt[2,4], Viacheslav O. Nikolaev[2,4‡], Lars S. Maier[3], Lars Klinge[1§], and Sven Thoms [1,2*]

[1]Department of Child and Adolescent Health, University Medical Center Göttingen, Robert-Koch-Straße 40, 37075 Göttingen, Germany; [2]DZHK (German Center for Cardiovascular Research), Partner Sites Göttingen and Hamburg, Germany; [3]Department of Cardiology, University Hospital Regensburg, Regensburg, Germany; [4]Institute of Pharmacology and Toxicology, University Medical Center Göttingen, Göttingen, Germany; and [5]Department of Cardiology and Pneumonology, University Medical Center Göttingen, Göttingen, Germany

Received 23 October 2019; revised 27 January 2020; editorial decision 31 March 2020; accepted 3 April 2020; online publish-ahead-of-print 23 June 2020

Aims The multi-C2 domain protein dysferlin localizes to the T-Tubule system of skeletal and heart muscles. In skeletal muscle, dysferlin is known to play a role in membrane repair and in T-tubule biogenesis and maintenance. Dysferlin deficiency manifests as muscular dystrophy of proximal and distal muscles. Cardiomyopathies have been also reported, and some dysferlinopathy mouse models develop cardiac dysfunction under stress. Generally, the role and functional relevance of dysferlin in the heart is not clear. The aim of this study was to analyse the effect of dysferlin deficiency on the transverse–axial tubule system (TATS) structure and on Ca^{2+} homeostasis in the heart.

Methods and results We studied dysferlin localization in rat and mouse cardiomyocytes by immunofluorescence microscopy. In dysferlin-deficient ventricular mouse cardiomyocytes, we analysed the TATS by live staining and assessed Ca^{2+} handling by patch-clamp experiments and measurement of Ca^{2+} transients and Ca^{2+} sparks. We found increasing co-localization of dysferlin with the L-type Ca^{2+}-channel during TATS development and show that dysferlin deficiency leads to pathological loss of transversal and increase in longitudinal elements (axialization). We detected reduced L-type Ca^{2+}-current ($I_{Ca,L}$) in cardiomyocytes from dysferlin-deficient mice and increased frequency of spontaneous sarcoplasmic reticulum Ca^{2+} release events resulting in pro-arrhythmic contractions. Moreover, cardiomyocytes from dysferlin-deficient mice showed an impaired response to β-adrenergic receptor stimulation.

Conclusions Dysferlin is required for TATS biogenesis and maintenance in the heart by controlling the ratio of transversal and axial membrane elements. Absence of dysferlin leads to defects in Ca^{2+} homeostasis which may contribute to contractile heart dysfunction in dysferlinopathy patients.

Keywords Dysferlin • Excitation–contraction coupling • Transverse–axial tubule system • Calcium transients • Muscular dystrophy

* Corresponding author. Tel: +49 551 39 62268. *E-mail address*: sven.thoms@med.uni-goettingen.de

† The first two authors contributed equally to the study.

‡ Present address. Institute for Experimental Cardiology, University Medical Center Hamburg, Hamburg, Germany.

¶ Present address. Computational and Systems Biology, Genome Institute of Singapore, Singapore, Singapore.

§ Present address. Kinderarztpraxis Göttingen, Göttingen, Germany.

What's new?

- Dysferlin is essential for transverse–axial tubule system (TATS) structure in the heart and dysferlin loss leads to rearrangement of TATS elements in a mouse model of dysferlinopathy.
- Dysferlin deficiency leads to defective Ca^{2+} homeostasis with decreased L-type Ca^{2+} current, reduced sarcoplasmic reticulum (SR) Ca^{2+} content, increased SR Ca^{2+} leak, and increased pro-arrhythmic events.
- In our model, dysferlin is anchored to the plasma membrane and in the TATS membrane. Dysferlin structures intracellular membranes by binding through C2 domains, thereby shaping the TATS structure in cardiomyocytes and supporting functional excitation–contraction coupling. When dysferlin is missing, TATS morphology is altered with loss of transversal elements, explaining dysregulated Ca^{2+} homeostasis.

Introduction

Dysferlin, a multi-C2 domain tail-anchored protein mainly expressed in skeletal muscle, is known for its role in Ca^{2+}-dependent membrane repair.[1,2] We and others have recently suggested that dysferlin is required in the biogenesis and maintenance of the T-tubule system in skeletal muscle.[1,3,4] Far less is known about the function of dysferlin in the heart muscle. Dysferlinopathy is a rare disease with an estimated incidence between 1/100 000 and 1/200 000. The disease, resulting from the lack of dysferlin protein due to recessive mutations in the *DYSF* gene, is mainly considered a skeletal muscle disease because only a few patients suffer from cardiomyopathy.[5,6] In those patients, dilated cardiomyopathy and electrocardiogram abnormalities have been reported.[7,8] Only a few studies looked at cardiac histology and found cardiac disarray and fibrosis. A large study on cardiac function in dysferlinopathy patients evaluated 48 patients and found prolonged QRS duration in 19 of 48 patients as well as disarray and fibrotic areas in histological sections.[5] Background conditions like age of disease onset and disease duration varied between patients. However, dysferlin is involved in membrane repair of cardiomyocytes and exhibits a cytoprotective function in an experimental model of ischaemia/reperfusion injury.[9,10] Under normal conditions, mouse models of dysferlin deficiency show either no or only mild cardiac phenotypes.[6,11] Excessive strains such as ischaemia/reperfusion injury, physical stress exercise, or β-adrenergic receptor (β-AR) activation by isoprenaline (ISO) provoke signs of cardiac dysfunction in dysferlinopathy mice.[6,9–13] Stress phenotypes show indications of membrane damage,[9,10] e. g. release of creatine kinase and Evans Blue dye uptake and include cardiac fibrosis, reduced fractional shortening (FS),[6,11] as well as decreased stroke volume and relaxation velocity.[12] Thus, systolic and diastolic cardiac functions can be altered upon stress in dysferlin-deficient mice.

Ventricular cardiomyocytes have a tubular membrane system which was initially thought to consist of exclusively transverse orientation relative to the contractile fibres of the myocyte. In the 1970s, axially orientated membrane structures were found in ventricular cardiomyocytes, interconnecting transverse membranes within the cytoplasm.[14] This highly complex system of elongated membrane tubules is termed transverse–axial tubule system (TATS).[15] The cardiac TATS is altered in heart failure (HF). The myocardium of HF patients displayed redistribution of the TATS with dilated and mainly longitudinally orientated tubules.[16] H F is characterized by diminished cardiomyocyte contraction resulting from uncoupling of L-type Ca^{2+}-channel—Ryanodine Receptor (LTCC/Ca_V1.2—RyR2) dyads and reduced systolic Ca^{2+} release.[17] Several studies suggest that the disturbed Ca^{2+} handling might result in part from the morphological abnormalities of the TATS.[18] Loss and redistribution of the transverse tubules (T-tubules) starts early in compensated hypertrophy before progression to HF.[19] Ca^{2+} release is delayed and asynchronous in cardiomyocytes from patients with HF.[20]

In this study, we analysed the expression of dysferlin during the development of healthy cardiomyocytes, as well as the TATS structure in dysferlin-deficient cardiomyocytes and the effects of dysferlin deficiency on cardiac Ca^{2+} homeostasis. Dysferlin is expressed in cardiomyocytes and localizes at the Z-lines and the TATS. Co-localization analysis revealed a spatial overlap of dysferlin and LTCC during cardiac TATS maturation. We found that the cardiac TATS is highly disorganized in dysferlin deficiency, including pathological axialization of membrane structures. We identified a decreased LTCC current ($I_{Ca,L}$), increased spontaneous sarcoplasmic reticulum (SR) Ca^{2+} release frequency and spontaneous cellular arrhythmias in dysferlin-deficient cardiomyocytes. Importantly, myocytes from dysferlin-deficient mice also showed impaired response to β-AR stimulation with decreased Ca^{2+} transients (CaT), decreased SR Ca^{2+} content and increased SR Ca^{2+} leak. Taken together, we suggest that dysferlin is essential for TATS formation and maintenance, and that dysferlin deficiency can manifest as functional Ca^{2+}-handling abnormalities in the heart.

Methods

Animals

DYSF gene-deleted C57/BL6 mice, *Dysftm1*^{Kcam}/*Dysftm1*^{Kcam}, were kindly provided by Professor Kate Bushby, Newcastle University, UK, with approval of the Mutant Mouse Regional Resource Centers (MMRRC), USA. In these mice, the last three coding exons including the exon coding for the transmembrane domain of the dysferlin gene were deleted leading to loss of expression of the dysferlin full-length protein. Heart and body weight was determined in mice used for Ca^{2+} measurements. Heart weight/body ratio was calculated as indicator for hypertrophy. Mice were 50–60 weeks old at the time of most experiments. Wistar WI rats used for isolation of cardiomyocytes and western blots of heart tissue were purchased from Charles River. All animal experiments were approved by the Niedersachsen animal review board (LAVES).

Disease models

Transaortic constriction (TAC) was done in 12 weeks old mice. The intervention was performed by tying a braided 5-0 polyviolene suture (Hugo Sachs Electronik) ligature around the aorta and a blunted 26-gauge needle and subsequent removal of the needle. For sham controls, the suture was not tied. To determine the level of pressure overload by aortic ligation, a high-frequency Doppler probe was used to measure the ratio between blood flow velocities in right and left carotid arteries. TAC mice with blood flow gradient <60% were excluded. For echocardiography, mice were anaesthetized by 2.4% isoflurane inhalation and ventricular measurements were done with a VisualSonics Vevo 2100 Imaging System equipped

with a MS400, 30 MHz MicroScan transducer. The observer was unaware of the genotypes and treatments. All these procedures were performed by the SFB 1002 S01 Disease Models service unit. Myocardial infarction (MI) was induced by ligation of the left anterior descending coronary artery of male, adult Sprague-Dawley rats and cardiomyocytes were isolated from the left ventricle of hearts 16-week post-MI.

Isolation of mouse ventricular cardiomyocytes

Hearts from male wild-type and dysferlin-null mice were excised after isoflurane anaesthesia and following cervical dislocation. Cardiomyocytes were isolated by Langendorff perfusion.[21] In brief, hearts were mounted on a Langendorff perfusion apparatus by cannulating the aorta and perfused with Ca^{2+}-free Tyrode's solution (140 mmol/L NaCl, 5.4 mmol/L KCl, 1 mmol/L $MgCl_2$, 5 mmol/L HEPES, 10 mmol/L Glucose, pH 7.54) for 6 min at 37°C. Perfusion was then switched to the same solution containing 0.8 mg/ml collagenase, with perfusion continuing until the heart became flaccid (~7–12 min). The ventricular tissue was then dispersed and filtered. Isolated cardiomyocytes were allowed to settle for 7 min, the supernatant was discarded and the cells were resuspended in Tyrode's solution containing 0.1 mmol/L Ca^{2+} and were settled again. This step was repeated with isolation solution containing 0.2 mmol/L, 0.4 mmol/L, 0.8 mmol/L, and 1.6 mmol/L Ca^{2+} for slow Ca^{2+} reintroduction.

Isolation of rat ventricular cardiomyocytes

Ventricular cardiomyocytes from 11-, 14-, 17-, 20-, 23-day-old or adult rats were isolated by retrograde perfusion of the heart according to the Langendorff technique after isoflurane anaesthesia and following cervical dislocation. Hearts were perfused with 8 mL/min at 37°C. After initial perfusion with Ca^{2+}-free buffer (NaCl 120.4 mmol/L, KCl 14.7 mmol/L, KH_2PO_4 0.6 mmol/L, $Na_2HPO_4 \times 2\ H_2O$ 0.6 mmol/L, $MgSO_4 \times 7\ H_2O$ 1.2 mmol/L, HEPES 10 mmol/L, $NaHCO_3$ 46 mmol/L, taurin 30 mmol/L, butanedione monoxime 10 mmol/L, glucose 5.5 mmol/L, pH 7.4) for 2 min, hearts were digested with collagenase type II (2 mg/mL, approximately 300 U/mg) and 40 µmol/L $CaCl_2$ in perfusion buffer for 9 min at 37°C. Following perfusion, the ventricles were separated from the atria and minced in digestion buffer. The tissue was carefully resuspended with a 10 mL serological pipette and the digestion process was stopped by adding stop buffer (FCS 10%, $CaCl_2$ 0.0125 mmol/L in perfusion buffer) before resuspending again. The cardiomyocytes were washed three times with stop buffer. Thereafter, cells were allowed to sediment by gravity for 8 min at room temperature.

Immunofluorescence staining of mouse cardiomyocytes

For immunofluorescence staining of cardiomyocytes, cells were seeded on laminin-coated cover slips and incubated for 1 h at room temperature or 30 min at 37°C. Mouse cells were fixed with ice-cold 100% ethanol at −20°C for 20 min and washed 3 × 5 min with cold PBS. Cells were incubated with blocking solution (5% BSA, 0.5% Triton X-100 in PBS) for 1 h. Rat cardiomyocytes were fixed in 4% PFA for 5 min at room temperature and blocked in 5% horse serum and 0.2% Triton X-100 for 1 h at room temperature. Mouse and rat cells were then incubated with the first antibody diluted in blocking solution at 4°C overnight. Cells were washed with PBS 3 × 10 min, incubated with the second antibody diluted in blocking solution for 1.5 h at room temperature and mounted with Vectashield mounting medium. Cells were imaged by confocal microscopy. Dysferlin was detected by anti-dysferlin antibody (NCL-Hamlet, Novocastra) and LTCC by anti-LTCC α1C/D/F/S (D-19, sc-10388, Santa Cruz Biotechnology).

Membrane staining of mouse ventricular cardiomyocytes with di-8-ANEPPS and analysis of transverse–axial tubule system morphology

Cells were gently resuspended in Tyrode's solution containing 50 µmol/L di-8-ANEPPS. Cells were immediately seeded in laminin-coated microscopy cell dishes (µ-dish, 35 mm, glass bottom, ibiTreat) and incubated for 30 min at room temperature in the dark. After washing once, cells were imaged by a Zeiss 710 NLO laser scanning microscope equipped with a 63×/1.4 NA oil objective. Analysis and image processing was done using Fiji (http://fiji.sc/) according to Ref.[22] with minor changes: For background subtraction, the rolling ball radius was set to 15. A ROI including intracellular TATS components and excluding plasma membrane and nuclei was set and further processed by background subtraction, contrast adjustment, smoothing, and segmentation. After same threshold setting was applied to all images during analysis. Cell area, normalized skeleton length, normalized number of structures, normalized number of branches, average branch length, and normalized number of endpoint voxels were determined from binary images by the Fiji plugin Analyze Skeleton (2D/3D). Using the Fiji plugin 'Directionality' the orientation of TATS components was assessed by quantifying the amount of structures for each direction (−45° to 134°) based on the two-dimensional skeletonized images. Quantification data was represented as a histogram with the amount of structures plotted against the structure direction. The amount of axial and transversal structures was calculated as the sum of structures with an orientation of −5° to +5° (axial) and +85° to +95° (transversal). T-tubule patterns were analysed by Fast Fourier transform (Image J) using regions of interest from skeletonized two-dimensional images.

Dysferlin protein and mRNA expression

Eleven-week-old rats were anaesthetized by isoflurane and sacrificed by cervical dislocation. 14-, 17-, 20-, 23-week-old rats and adult rats were euthanized by carbon dioxide inhalation and immediate opening of the thorax. The ventricular part of the heart was separated from the atrial part, transferred into reaction tubes and frozen in liquid nitrogen. After thawing on ice, the cardiac tissue was homogenized five times for 5 s. The homogenate was centrifuged two times at 1300×*g* for 10 min at 4°C and in between centrifugation steps, the supernatant was transferred into a new reaction tube. Mouse hearts were homogenized in a hypotonic buffer containing 10 mmol/L HEPES, 10 mmol/L KCl, 2 mmol/L $MgCl_2$, 0.1 mmol/L EDTA, and 1 mmol/L DTT with protease inhibitors. After 10 min ice incubation, NP-40 was added to a final concentration of 1% followed by 5 min ice incubation. Lysates were centrifuged at 4000 rpm for 5 min at 4°C. Supernatants were used for Western blot. Rat heart tissue after MI was homogenized in RIPA buffer containing 150 mmol/L NaCl, 5 mmol/L EDTA pH 8.0, 50 mmol/L Tris, pH 8.0, 1% NP-40, 0.5% sodium deoxycholate, 0.1% SDS, and protease and phosphatase inhibitors. Dysferlin was detected in homogenates of the ventricular heart tissue of rats and mice by Western blot using anti-dysferlin antibody . Anti-GAPDH or anti-tubulin antibody was used as loading control (G8795 or T8203, Sigma-Aldrich).

Mouse ventricular tissue was macrodissected and used for RNA isolation. RNA was isolated using NucleoSpin Tissue genomic DNA and RNA kit (Macherey-Nagel), respectively, as described elsewhere.[1] Nucleic acid quantification was assessed using a Nanodrop photometer (Thermo Scientific). 500 ng RNA was used for cDNA synthesis using 0.5 µg Oligo(dT)20 primer and 100 U M-MLV reverse transcriptase (Promega) for 1 h at 42°C. Quantitative real-time PCR (qPCR) analyses were performed with SYBR Green (Promega) on a 7900-HT Real-time cycler (Applied Biosystems) using primers for dysferlin (for:

CACCTTGCCTGCGATGTTTC, rev: CCAGGTTGTCGTCCACT TCT) and Tbp (for: CCAGAACAACAGCCTTCCACC, rev: CAA CGGTGCAGTGGTCAGAGT). Gene expression was normalized to Tbp. Copy numbers were calculated using the SDS2.4 software with a relative standard curve obtained using the log dilutions of cDNA of gene of interest. All reactions were run in triplicates and normalized to reference control genes.

Expression of dysferlin mRNA in human, mouse, and rat

For analysis of expression of dysferlin transcripts in brain, cerebellum, heart, kidney, liver, ovary, and testes, postnatal expression data from Cardoso-Moreira *et al.*[23] in these tissues were averaged and reads per kilobase million values were plotted without normalization.

Simultaneous measurement of $I_{ca,L}$ and intracellular Ca^{2+} concentrations

LTCC($I_{Ca,L}$) were recorded in whole-cell ruptured-patch configuration using voltage-clamp technique in Fluo-3 AM (ThermoFisher; 10 µmol/L, 10 min loading and 30 min de-esterification) loaded cells for simultaneous measurement of intracellular Ca^{2+} concentration ($[Ca^{2+}]i$). Seal-resistances were 4–8 GΩ. Resistance and cell capacitance were compensated. During experiments, myocytes were superfused at 37°C with a bath solution containing (in mmol/L): $CaCl_2$ 2, glucose 10, HEPES 10, KCl 4, $MgCl_2$ 1, NaCl 140, probenecid 2; pH = 7.4. In addition, Fluo-3 was included into the pipette solution containing (in mmol/L): EGTA 0.02, Fluo-3 0.1 (Invitrogen), GTP-Tris 0.1, HEPES 10, potassium aspartate 92, KCl 48, Mg-ATP 1, Na_2-ATP 4; pH 7.2. $I_{Ca,L}$ was activated using a holding potential of −80 mV and a 500-ms ramp pulse to −40 mV to inactivate the fast Na^+-current followed by a depolarizing step to +10 mV for 100 ms (sweep interval 2 s). pClamp-Software (V10.2, Molecular Devices, Sunnyvale, CA, USA) was used for data acquisition and analysis. Currents are expressed as densities (pA/pF). Membrane capacitance was similar in wild-type and dysferlin-deficient myocytes. Fluorescence was excited at 488 nm and emitted light (<520 nm) converted to $[Ca^{2+}]_i$ assuming

$$[Ca^{2+}]_i = k_d\left(\frac{F}{F_{max} - F}\right)$$

Where k_d = dissociation constant of Fluo-3 (864-nmol/L), F = Fluo-3 fluorescence; F_{max} = Ca^{2+} saturated fluorescence obtained at the end of each experiment. Drugs were applied *via* a rapid-solution exchange system.

Cell shortening and intracellular Ca^{2+} measurements

Detection of CaT was carried out by epifluorescence microscopy (ION OPTIX) at 37°C. The chamber was perfused with a constant flow of 80 mL/h of Tyrode's solution with 1 mmol/L Ca^{2+}. Excess dye was removed from the chambers and cells were stimulated at 1 Hz to achieve a steady state. Fluo-4 acetomethyl ester (AM) was excited at 488 nm using a 75 W xenon arc lamp on stage of a Nicon Eclipse TE 200-U inverted microscope. Emitted fluorescence at 535 nm was measured using a photomultiplier and shortening of the cells was measured using a sarcomere length detection system (Ion Optix Corp, Milton, MA, USA). CaT amplitudes and shortening of the cells were measured at 0.5, 1, 2, 3, and 4 Hz. After subtraction of background fluorescence, F/F0 was calculated by dividing raw fluorescence (F) by baseline fluorescence (F0). For measurement of SR Ca^{2+} content stimulation was stopped for 30 s and CaT before and after rest were analysed (post-rest relation). For β-AR stimulation protocols, cells were provided with a constant flow of Tyrode's solution with ISO (10^{-7} mol/L). For measurement of SR Ca^{2+}, stimulation was stopped and addition of Tyrode's solution with caffeine (10 mmol/L) evoked Ca^{2+} release from the SR. Analysis of CaT and shortening was done with IONWizard Analyze Version 5.0 (Ion Optix). Fractional Ca^{2+} release (FR) was calculated as the ratio between CaT amplitude and caffeine transient amplitude (SR Ca^{2+} load) measured in the same cardiomyocyte. Analysis of non-stimulated events was done using the following semi-quantitative arrhythmia score: single non-stimulated event: 1 point, bigeminy or trigeminus (coupled non-stimulated event): 2 points, couplet (two following non-stimulated events): 3 points, triplet (three following non-stimulated events): 4 points, salvo (four or more following non-stimulated events): 5 points, tachycardia (non-stimulated events following for more than 10 s): 6 points.

Ca^{2+} spark measurements

Cells were seeded on laminin-coated chambers and incubated for 15 min at room temperature. Cells were then incubated with 10 µmol/L of Fluo-4 AM in the dark at room temperature. Incubation time was 20 min for Ca^{2+} measurements and 7 min for spark measurements. Detection of Ca^{2+} sparks was done at room temperature by laser scanning confocal microscopy (LSM 5 Pascal, Zeiss) using a 40× oil-immersion objective. Fluo-4 AM was excited with an argon laser at 488 nm and emitted fluorescence was collected through a 515 nm long-pass filter. Cells were measured with 0.25 Hz stimulation and after an unstimulated period of 30 s. Measurements were done in 'line-scan'-mode with a pixel time of 0.8 µs, a scan time of 960 µs, 510 pixel per line, a pixel size of 0.1 µm, a pixel depth of 12 bit, a scan width of 51 µm (zoom factor 4.5) and 4000 lines. Analysis of spark measurements was done using Image J plug in Sparkmaster. Ca^{2+} spark frequency (CaSpF) was normalized to cell width and scan time ($\mu m^{-1} * s^{-1}$). Peak of Ca^{2+} sparks was normalized to F/F0 (the raw fluorescence was divided by the baseline fluorescence after subtraction of the background fluorescence). Duration of sparks was taken from the full-duration half maximum (FDHM) and width of the sparks from the full-width half maximum (FWHM). The Ca^{2+} spark volume was calculated from duration, width and amplitude of the sparks. Ca^{2+} spark-derived SR Ca^{2+} leak (µmol/L cytosol/s) was calculated as following: After calibration of F/F0 by using the equation $[Ca]_i = K_d\ (F/F_0)/(K_d/[Ca]_{i\text{-}rest} + 1 - F/F_0)$ (with K_d = 1100 nmol/L and $[Ca]_{i\text{-}rest}$ = 100 nmol/L), Ca spark flux (J) was calculated as J = B Δ$[Ca^{2+}]$*V*T-1 with B being the buffering power of Fluo, V being the volume occupied by a spark, and T being the time taken for rise of Ca^{2+}. The Ca^{2+} spark flux was integrated as a function of time for each spark, which corresponds to the amount of Ca^{2+} released by this spark. Thereafter, the sum of all Ca^{2+} released by the sparks during the line scan was calculated and normalized to the cytosolic volume scanned during the line scan and scan time. The cytosolic volume was calculated from cell width according to.[24] For induction of β-AR stress, the cells were provided with a constant flow of Tyrode's solution with ISO. For calibration of Fluo-4, F_{max} was measured by exposing the cells to 10 µmol/L ionomycin in presence of 10 mmol/L $MnCl_2$ to saturate fluorescence. F_{max} was calculated as $F_{max} = 5 \times F_{Mn}$ and F_{min} was calculated as $F_{min} = 1/40\ F_{max}$. $[Ca]_i$ was calculated using a K_d value of 864 nm and $[Ca]_i$ was calculated as $[Ca]_i = K_d \times (F - F_{min})/(F_{max} - F)$.

Statistical analyses

Statistical analysis was done with Excel or GraphPad Prism 8 by Student's *t*-test or two-way analysis of variance (ANOVA) for repeated measurements. When multiple cells per mouse were measured nested ANOVA or nested *T*-tests were performed. Data were checked for normal distribution. *P*-values less than 0.05 were considered statistically significant. If not stated otherwise, data are shown as box plots with median and individual data points (box represents the 95% confidence interval, whiskers show minimum and maximum values).

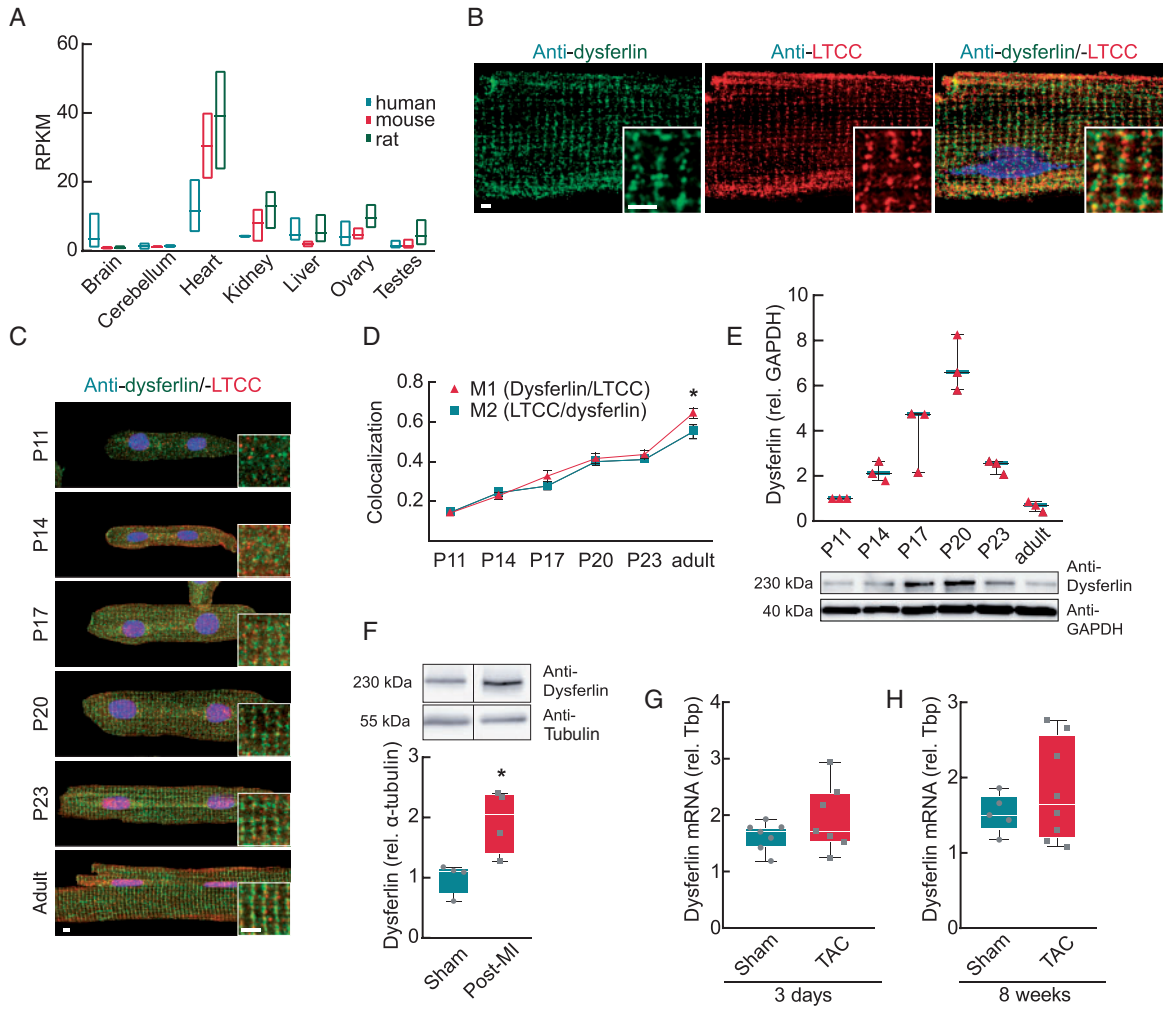

Figure 1 Dysferlin localizes to the cardiac TATS and is up-regulated during biogenesis and regeneration. (*A*) Dysferlin mRNA expression in human, mouse, and rat heart. Averages of postnatal transcript expression of between four and eight time points after birth.[23] (*B*) Cardiomyocytes from 20 weeks old mice were stained with antibodies against dysferlin and L-type Ca^{2+} channel (LTCC, $Ca_V1.2$). Cells were analysed by fluorescence microscopy and z-stacks were deconvolved. Scale bar: 2.5 µm. (*C* and *D*) Dysferlin is expressed during TATS biogenesis and localizes to the developing TATS in cardiomyocytes. Isolated ventricular rat cardiomyocytes (P, days after birth) were co-stained with antibodies against dysferlin (green) and the LTCC (red). DAPI staining is shown in blue. Cells were imaged by confocal microscopy. Scale bar: 2.5 µm. (*D*) Co-localization of dysferlin and LTCC increases during the biogenesis of the TATS. Co-localization of dysferlin and LTCC was determined by Manders coefficients M1 and M2. $N = 3$ mice and 15 cells per group, $^*P \leq 0.05$. Mean ± SEM. (Student's *t*-test). (*E*) Protein expression of dysferlin was analysed by western blot using ventricular heart muscle homogenates from rats of corresponding ages. Dysferlin expression peaks at P20. $N = 3$ rats per age group. (*F*) Dysferlin is up-regulated after MI. MI was induced in rat hearts by ligation of the left coronary artery. Sixteen weeks post-MI protein levels of ventricular heart muscle homogenates were determined and normalized to tubulin. Protein levels of MI hearts were then normalized to sham hearts. $^*P < 0.05$, $N = 4$ per group (Student's *t*-test). (*G* and *H*) Dysferlin mRNA expression in ventricular heart muscle from mice 3 days (*G*) or 8 weeks (*H*) after TAC or sham operation relative to Tbp. Dysferlin mRNA is not significantly increased after TAC. $N = 7$ mice. MI, myocardial infarction; TATS, transverse-axial tubule system; Tbp, TATA-binding protein.

Results

Dysferlin localization and expression in transverse–axial tubule system biogenesis

Dysferlin is highly expressed in the heart in human, mouse, and rat (*Figure 1A*). In the cardiac muscle, dysferlin has been found localized at the sarcolemma (plasma membrane), the intercalated disks, and the T-tubular membrane.[11,12] We analysed dysferlin localization by immunofluorescence in isolated cardiomyocytes of wild-type mice with antibodies against dysferlin and the LTCC. We found that dysferlin localized to TATS and co-localizes with LTCC (*Figure 1B*).

As dysferlin is crucial for maintenance of TATS structure, we next aimed to study dysferlin expression during cardiac and TATS

development. Therefore, isolated ventricular cardiomyocytes from rats of different ages were co-stained with antibodies against dysferlin and LTCC to visualize TATS formation. Co-localization of both proteins increased from postnatal day 11 (P11) to day 23 (P23), the time slot of TATS formation and was highest in the adult rat (*Figure 1C and D*). Protein levels detected in ventricular homogenates from rat hearts of the corresponding ages showed a 7-fold increase in dysferlin protein level from P11 to P20 and a decreased expression in adulthood (*Figure 1E*). Protein and mRNA levels in ventricular mouse heart homogenates showed an increased expression of dysferlin from embryonic day 14.5 (E14.5) to adulthood (Supplementary material online, *Figure S1A* and *B*). These results indicate a convergent localization of dysferlin and LTCC during cardiac development.

During HF development a process of progressive membrane remodelling takes place. Hence, we aimed to study if pathological cardiac remodelling could affect not only TATS but also dysferlin. Myocardial infarction (MI) was induced in rat hearts by ligating the left coronary artery inducing membrane remodelling. Surprisingly, dysferlin protein levels were significantly up-regulated 16 weeks after MI (*Figure 1F*). In contrast, we did not find significant changes of dysferlin mRNA in mouse hearts 3 days or 6 weeks after TAC (*Figure 1G and H*).

Dysferlin is essential for transverse–axial tubule system structure in the heart

We aimed to analyse TATS structure in the dysferlin-deficient heart using a mouse model containing a general knockout of dysferlin.[1] This model best represents the situation of the dysferlinopathy patients. Direct visualization of the TATS with the lipophilic dye di-8-ANEPPS in ventricular cardiomyocytes of dysferlin-deficient mice (*Figure 2A*) and structural analysis (*Figure 2B–F*) revealed dramatic changes in TATS organization in these mice. The distance between transverse TATS elements was measured after Fourier transform and shows a reduced regularity (*Figure 2B*). To assess the extent of structural changes of the entire TATS quantitatively, images were binarized and skeletonized (*Figure 2C*). The membrane skeleton was used to quantify the amount of membrane elements for each direction depicted as a histogram (*Figure 2D*). This analysis revealed a bimodal distribution, both, for dysferlin-deficient and control cells. However, cardiomyocytes of dysferlin-deficient mice show a significant shift from transverse to axial elements of TATS (axialization) (*Figure 2D and E*). Further characterization of the skeletonized images revealed that dysferlin-deficient cardiomyocytes contain less and shorter TATS structures per cell with diminished branching compared to wild-type cardiomyocytes (*Figure 2F*). Cell area and average branch length were not different (Supplementary material online, *Figure S2*). Thus, loss of dysferlin leads to dramatic reduction in the ratio of transverse and longitudinal elements, remodelling and an overall loss of TATS structural elements.

L-type Ca^{2+} current is reduced in dysferlin-deficient cardiomyocytes

As cardiac dysferlin is located in the TATS, co-localizes with LTCC and is possibly involved in T-tubule remodelling, we tested the hypothesis that loss of dysferlin affects Ca^{2+} homeostasis. We first measured $I_{Ca,L}$ using whole-cell patch-clamp technique together with simultaneous CaT measurement by epifluorescence. $I_{Ca,L}$ density was significantly decreased in dysferlin-deficient myocytes ($I_{Ca,L}$: $Dysf^{+/+}$ = 7.07 ± 0.79 pA/pF, $Dysf^{-/-}$ = 4.02 ± 0.82 pA/pF; Integrated $I_{Ca,L}$: $Dysf^{+/+}$ = 0.11 ± 0.01 pC/pF, $Dysf^{-/-}$ = 0.06 ± 0.01 pC/pF, N = 12 $Dysf^{+/+}$ and 5 $Dysf^{-/-}$ mice) (*Figure 3A and B* and Supplementary material online, *Figure S3A* and *B*) whereas amplitude, decay and time to peak of systolic CaT remained unaltered (*Figure 3C–E*).

Ca^{2+} transients and shortening are unchanged in dysferlin-deficient cardiomyocytes

To analyse whether the decreased $I_{Ca,L}$ has impact on cardiomyocyte contraction, we studied CaT and cell shortening in intact fluo-4-loaded isolated ventricular myocytes during field electrical stimulation (0.5–4 Hz). CaT amplitude and FS of dysferlin-deficient cardiomyocytes were not different from wild-type (*Figure 4A and B*). Also, time to peak and relaxation time (RT) were not altered (*Figure 4C and D*). These findings indicate no changes in cell contractility. Biometric data of dysferlin-deficient and wild-type mice did not show signs of overt cardiac hypertrophy (*Figure 4E*).

SR Ca^{2+} load determined by rapid application of caffeine was significantly decreased in dysferlin-deficient cardiomyocytes compared to wild-type cardiomyocytes (*Figure 4F, H*) indicating a decreased SR Ca^{2+} content ($Dysf^{+/+}$ = 4.76 ± 0.35 F/F0, $Dysf^{-/-}$ = 3.46 ± 0.27 F/F0, N = 7 mice per group). RT50 of caffeine-induced CaT in dysferlin-deficient cells were not different from wild-type (*Figure 4G and H*) indicating no change in sodium calcium exchanger (NCX) function if differences are not masked by other ion channels variations. Fractional release (FR) of SR Ca^{2+} in dysferlin-deficient cardiomyocytes was significantly increased to 66.71 ± 3.01% compared to 54.88 ± 4.60% (N = 7 mice per group) in wild-type cells (*Figure 4I*).

Taken together, dysferlin-deficient ventricular myocytes showed unaltered CaT amplitude and contractile function.

Beta-adrenergic stress unmasks further Ca^{2+} handling abnormalities in dysferlin-deficient cardiomyocytes

In contrast to unstressed conditions, we found a diminished enhancement of CaT after β-AR stimulation with ISO in dysferlin-deficient cardiomyocytes compared to wild-type ($Dysf^{+/+}$ = 5.15 ± 0.31 F/F0, $Dysf^{-/-}$ = 4.35 ± 0.24 F/F0, N = 7 mice per group) (*Figure 5A and C*). Time to peak and RTs were not significantly different after ISO treatment (*Figure 5B and D*). SR Ca^{2+} load was significantly decreased in dysferlin-deficient cardiomyocytes compared to wild-type cardiomyocytes after β-AR activation by ISO ($Dysf^{+/+}$ = 5.58 ± 0.63 F/F0, $Dysf^{-/-}$ = 3.98 ± 0.31 F/F0, N = 7 mice per group) (*Figure 5E and F*). RT50 of caffeine-induced CaT in dysferlin-deficient cells after ISO stimulation was not altered (*Figure 5E and F*). FR after β-AR stimulation was significantly increased in dysferlin-deficient myocytes ($Dysf^{+/+}$ = 83.33 ± 3.08%, $Dysf^{-/-}$ = 93.59 ± 2.06%, N = 7 mice per group) (*Figure 5G*).

Cardiomyocytes were electrically stimulated at 1 Hz and stimulation was then stopped for 30 s to detect post-rest cytosolic Ca^{2+}, a measure for SR Ca^{2+} loss. Post-rest CaT showed no differences between dysferlin-deficient and wild-type cardiomyocytes (Supplementary material online, *Figure S4A* and *B*). After β-AR stimulation, post-rest CaT

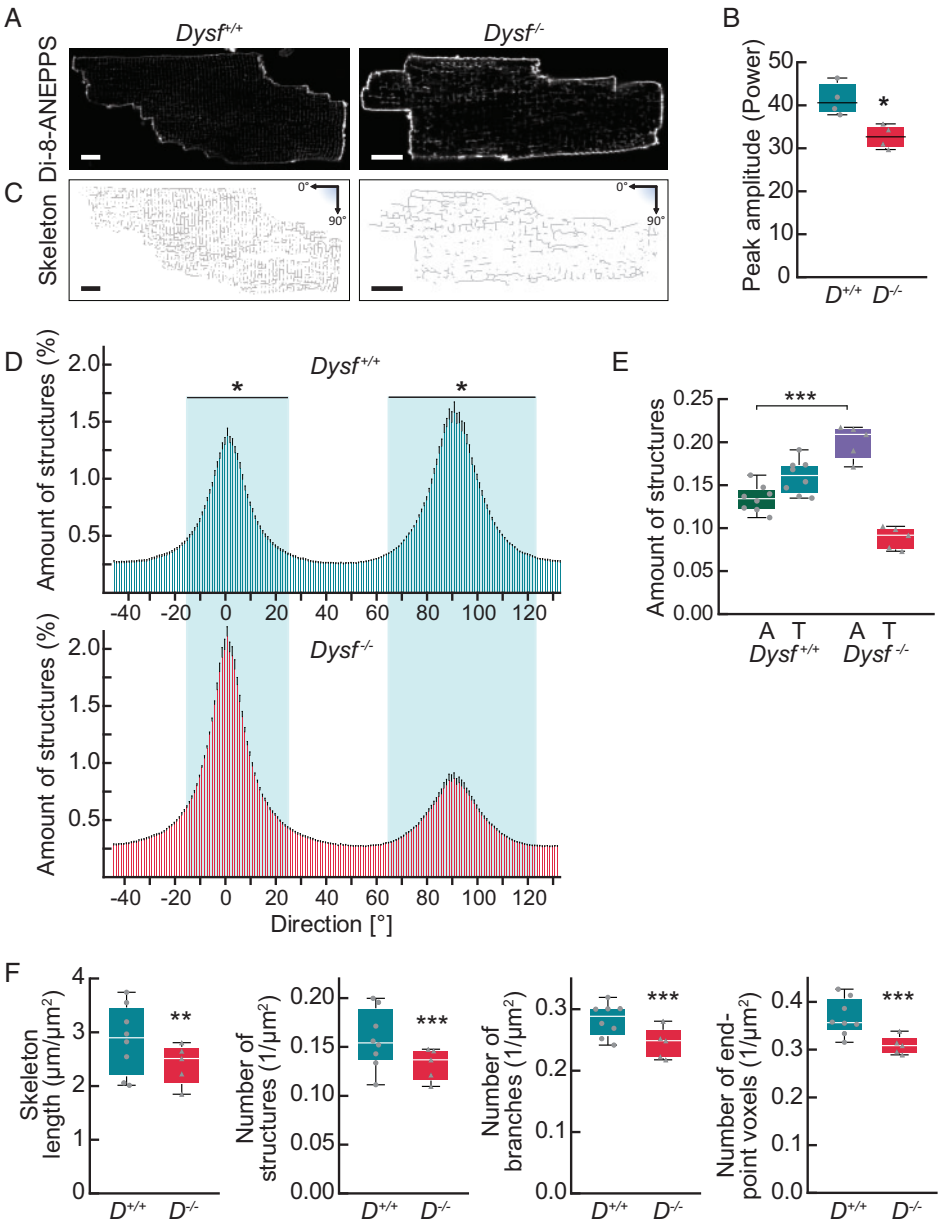

Figure 2 Loss of transverse elements in the TATS of dysferlin-deficient cardiomyocytes. (*A*) Ventricular cardiomyocytes from dysferlin-deficient ($Dysf^{-/-}$) and wild-type ($Dysf^{+/+}$) mice were isolated, stained with the membrane dye di-8-ANEPPS and analysed by confocal microscopy. Scale bar: 10 µm. (*B*) Fourier transform of di-8-ANEPPS-stained cardiomyocytes. *$P < 0.05$ (nested *t*-test) $N = 4$ mice. (*C–F*) Analysis of tubular membrane network in ventricular cardiomyocytes of dysferlin-deficient mice. The confocal image signal (*A*) was skeletonized (*C*) for subsequent detailed analysis of membrane structures. Scale bars: 10 µm. (*B–D*) Altered directionality of TATS in ventricular cardiomyocytes of dysferlin-deficient mice. (*D* and *E*) Quantification of structure directionality depicted as histograms with one bar for each direction. $N = 8$ ($Dysf^{+/+}$) and 5 ($Dysf^{-/-}$) mice (5–20 cells/mouse). Mean ± SEM. (*D*) $Dysf^{+/+}$ (green) and $Dysf^{-/-}$ (red). Light green boxes mark area of direction with significant differences between $Dysf^{-/-}$ and $Dysf^{+/+}$ for each bin [16–24°, 64–118°. *$P \leq 0.05$ (nested ANOVA)]. (*E*) Summed amount of structures with axial (A, 0° ± 5°) and transverse (T, 90° ± 5°) orientation. ***$P \leq 0.001$. (*F*) Altered structural parameters of TATS in ventricular cardiomyocytes of dysferlin-deficient mice. The following parameters were used to characterize the skeletonized TATS: normalized skeleton length, normalized number of structures, normalized number of branches, and normalized number of endpoint voxels. Skeleton length, number of structures, number of branches, and number of endpoint voxels were normalized to the cell area. $N = 8$ ($Dysf^{+/+}$) and 5 ($Dysf^{-/-}$) mice (5–20 cells/mouse). **$P \leq 0.01$, ***$P \leq 0.001$ (nested *t*-test). ANOVA, analysis of variance; TATS, transverse-axial tubule system.

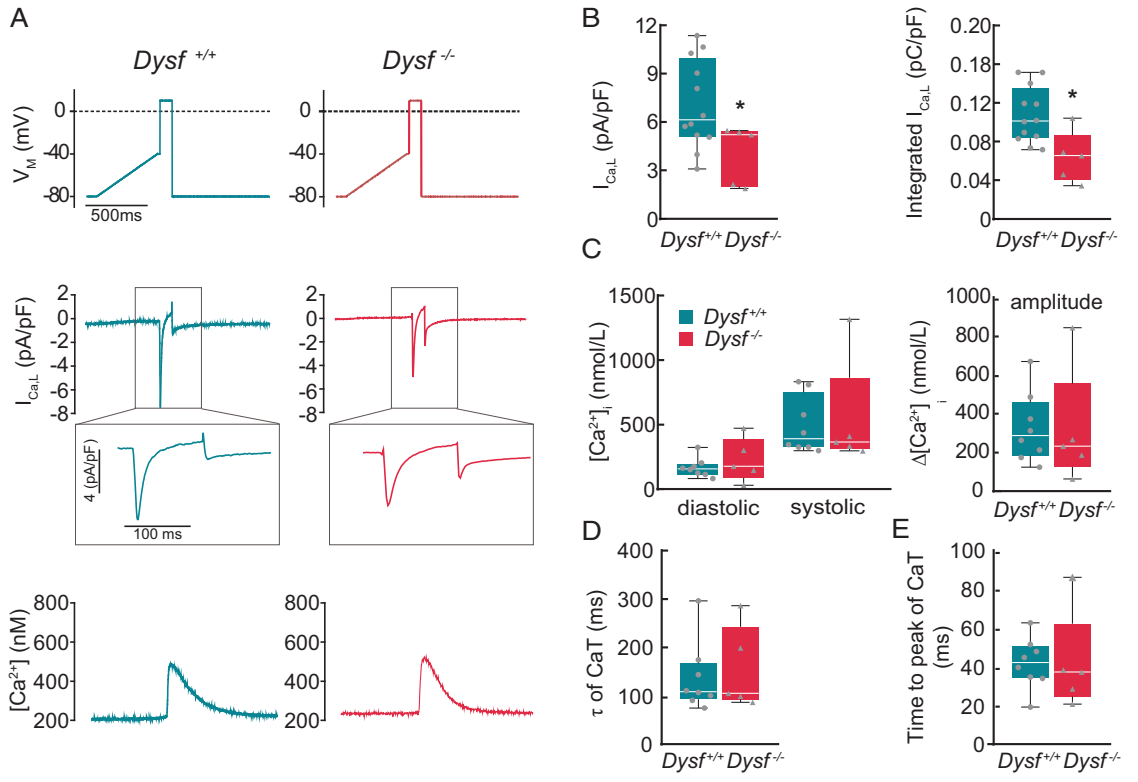

Figure 3 L-type calcium current ($I_{Ca,L}$) and corresponding triggered Ca^{2+} transients (CaT) in dysferlin-deficient cardiomyocytes. (*A*) Top: voltage-clamp protocol (0.5 Hz). V_M, membrane potential. Below: simultaneous recording of $I_{Ca,L}$ (middle) and triggered CaT (Fluo-3, bottom) in wild-type (left) and dysferlin-deficient (right) myocytes in presence of 2 mmol/L Ca^{2+}. (*B*) Peak-$I_{Ca,L}$ (left) and integrated $I_{Ca,L}$ (right). Mean $I_{Ca,L}$: $Dysf^{+/+}$ = 7.07 ± 0.79 pA/pF, $Dysf^{-/-}$ = 4.02 ± 0.82; pA/pF; mean integrated $I_{Ca,L}$: $Dysf^{+/+}$ = 0.11 ± 0.01 pC/pF, $Dysf^{-/-}$ = 0.06 ± 0.01 pC/pF. (*C*) Diastolic and systolic $[Ca^{2+}]_i$ (left) and resulting CaT amplitude (right). (*D*) Time-constant (τ) of decay of $I_{Ca,L}$-triggered CaT. (*E*) Time to peak of CaT. $N = 12$ ($Dysf^{+/+}$) and 5 ($Dysf^{-/-}$) mice. *$P \leq 0.05$ vs. wild-type (Student's *t*-test).

were significantly smaller in dysferlin-deficient myocytes ($Dysf^{+/+}$ = 6.18 ± 0.45 F/F0, $Dysf^{-/-}$ = 4.85 ± 0.34 F/F0, $N = 7$ mice per group) (Supplementary material online, *Figure S4A* and *B*).

Increased sarcoplasmic reticulum Ca^{2+} leak in dysferlin-deficient cardiomyocytes

Because cardiac remodelling and loss of TATS leads to disruption of the tight coupling between LTCC and RyR2 producing orphaned RyR2 clusters,[25] we wanted to study RyR2 function and further characterize SR Ca^{2+} leak in dysferlin-deficiency. Ca^{2+} spark frequency was significantly increased in dysferlin-deficient cardiomyocytes compared to wild-type ($Dysf^{+/+}$ = 0.65 ± 0.03 100 $\mu m^{-1}s^{-1}$, $Dysf^{-/-}$ = 1.88 ± 0.25 100 $\mu m^{-1}s^{-1}$, $N = 4$ mice per group) (*Figure 6A and B*) leading to a dramatically increased Ca^{2+} leak from the SR ($Dysf^{+/+}$ = $4.95 \times 10^{-5} \pm 9.40 \times 10^{-6}$ nmol/L, $Dysf^{-/-}$ = $1.16 \times 10^{-4} \pm 2.50 \times 10^{-5}$ nmol/L, $N = 4$ mice per group) (*Figure 6G* and Supplementary material online, *Figure S5*). Spark amplitude, duration, width and diastolic Ca^{2+} were not different in these cells (*Figure 6C–F*). β-AR stimulation using ISO lead to increased spark duration and width (*Figure 6A, D, and E*) compared to ISO stimulated wild-type cells thereby further increasing the Ca^{2+} leak in dysferlin-deficient cardiomyocytes ($Dysf^{+/+}$ = $1.47 \times 10^{-4} \pm 2.27 \times 10^{-5}$ nmol/L, $Dysf^{-/-}$ = $2.82 \times 10^{-4} \pm 4.05 \times 10^{-5}$ nmol/L, $N = 4$ mice per group) (*Figure 6G* and Supplementary material online, *Figure S5*).

To determine if this increase in Ca^{2+} spark frequency may lead to arrhythmia, we analysed the occurrence of spontaneous cellular contractions. We found small increase in pro-arrhythmogenic events in dysferlin-deficient cardiomyocytes under basal conditions (score/observation time: $Dysf^{+/+}$ = $9.31 \times 10^{-4} \pm 4.82 \times 10^{-4}$, $Dysf^{-/-}$ = $7.85 \times 10^{-3} \pm 4.04 \times 10^{-3}$, $N = 7$ mice per group) but significantly increased numbers after ISO treatment (Score/observation time: $Dysf^{+/+}$ = $2.67 \times 10^{-3} \pm 0.80 \times 10^{-3}$, $Dysf^{-/-}$ = $1.98 \times 10^{-2} \pm 0.70 \times 10^{-2}$, $N = 7$ mice per group) (*Figure 6H and I*). Increased spark frequency and SR Ca^{2+} leak together with increased pro-arrhythmogenic events may increase the risk of arrhythmias in dysferlin-deficient hearts, especially under β-AR stimulation.

Discussion

Dysferlin is highly expressed in heart muscle and the symptomatic spectrum of dysferlin deficiencies involves cardiomyopathies.[2,6,9] Thus, dysferlin plays a role in cardiac health, but it is not understood how dysferlin supports heart function and how lack of dysferlin

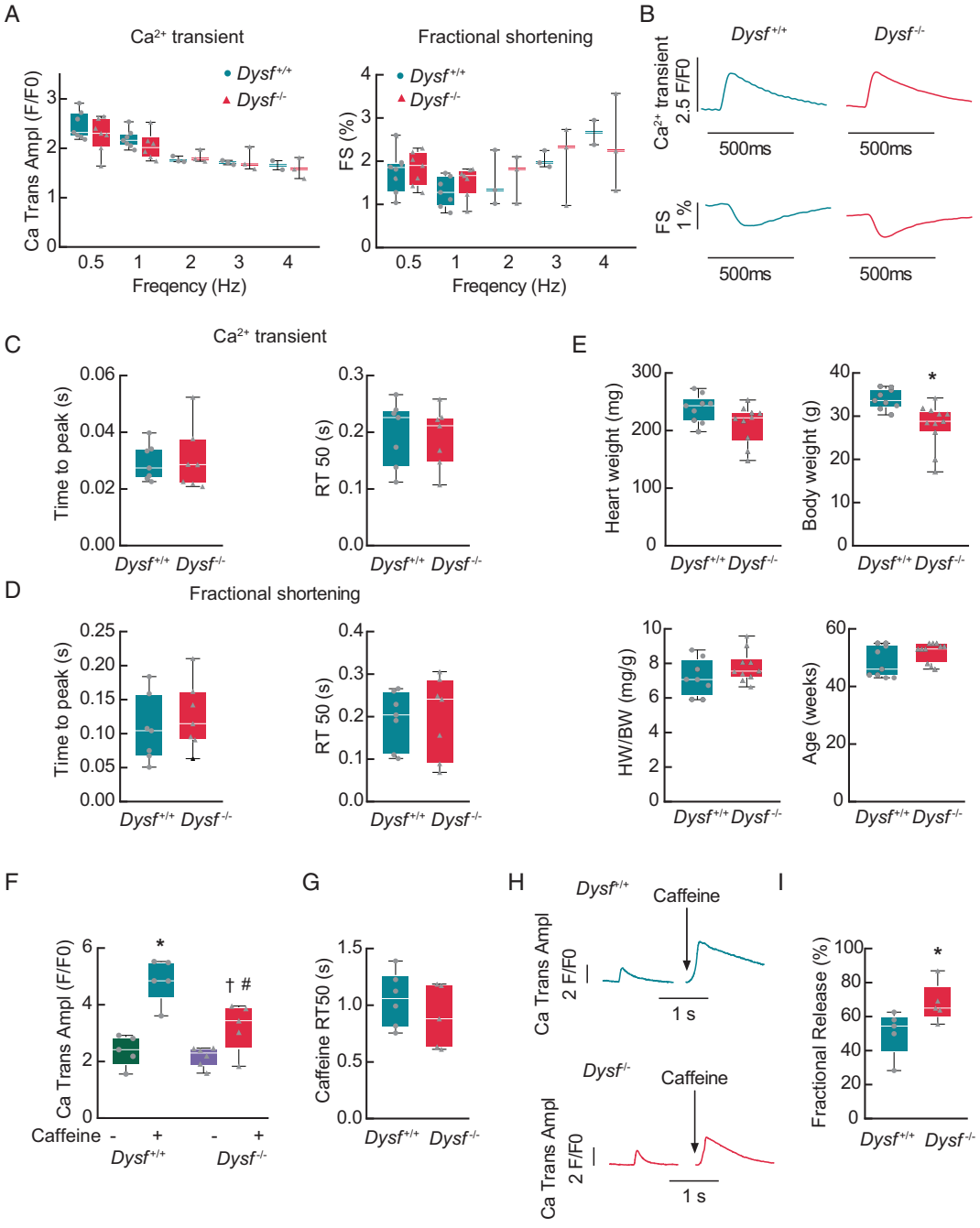

Figure 4 Decreased SR Ca^{2+} content but no signs of overt cardiac hypertrophy and cardiac dysfunction in dysferlin-deficient mice under physiological conditions. (*A–D*) Ca^{2+} release and fractional shortening (FS) of cardiomyocytes from male dysferlin-deficient ($Dysf^{-/-}$) mice are not altered under normal conditions. Isolated cardiomyocytes were loaded with fluo-4 and Ca^{2+} release and FS were detected after stimulation with 0.5–4 Hz in presence of 1 mmol/L Ca^{2+}. (*A*) Average CaT amplitudes and FS. (*B*) Representative steady-state (1 Hz) CaT amplitudes and FS of wild-type ($Dysf^{+/+}$) and knockout cardiomyocytes. (*C*) Time to peak and RT50 (50% relaxation time) of CaT amplitudes at 1 Hz. (*D*) Time to peak and RT50 of FS at 1 Hz. $N = 7$ mice and ≥8 cells. (*E*). Dysferlin-deficient mice do not show signs of overt cardiac hypertrophy. Dysferlin-deficient mice show reduced body weight (BW) compared to wild-type mice, but no difference in heart weight (HW) or HW/BW ratio. Age 50–60 weeks. $^{*}P \leq 0.05$ vs. wild-type, $N = 8$ mice per group (nested *t*-test). (*F–H*) Decreased SR Ca^{2+} content and unchanged RT in dysferlin-deficient cardiomyocytes. A 10 mmol/L caffeine was applied to isolated cardiomyocytes. Steady-state and caffeine-induced CaT amplitudes (*F*) and RT50 (*G*) of caffeine-induced CaT. Mean caffeine-induced CaT amplitudes: $Dysf^{+/+} = 4.76 \pm 0.35$ F/F0, $Dysf^{-/-} = 3.46 \pm 0.27$ F/F0. (*H*) Representative steady-state (1 Hz) and caffeine-induced CaT amplitudes. (*I*) Fractional release (FR) of SR Ca^{2+} content is significantly increased in dysferlin-deficient cardiomyocytes. Mean FR: $Dysf^{+/+} = 54.88 \pm 4.60\%$ and $Dysf^{-/-} = 66.71 \pm 3.01\%$ $^{*}P \leq 0.05$ vs. $Dysf^{+/+}$, $^{\#}P \leq 0.05$ vs. $Dysf^{+/+}$+Caff, $^{\dagger}P \leq 0.05$ vs. $Dysf^{-/-}$, nested *t*-test or nested ANOVA, $N = 5$ mice and ≥11 cells per group. ANOVA, analysis of variance.

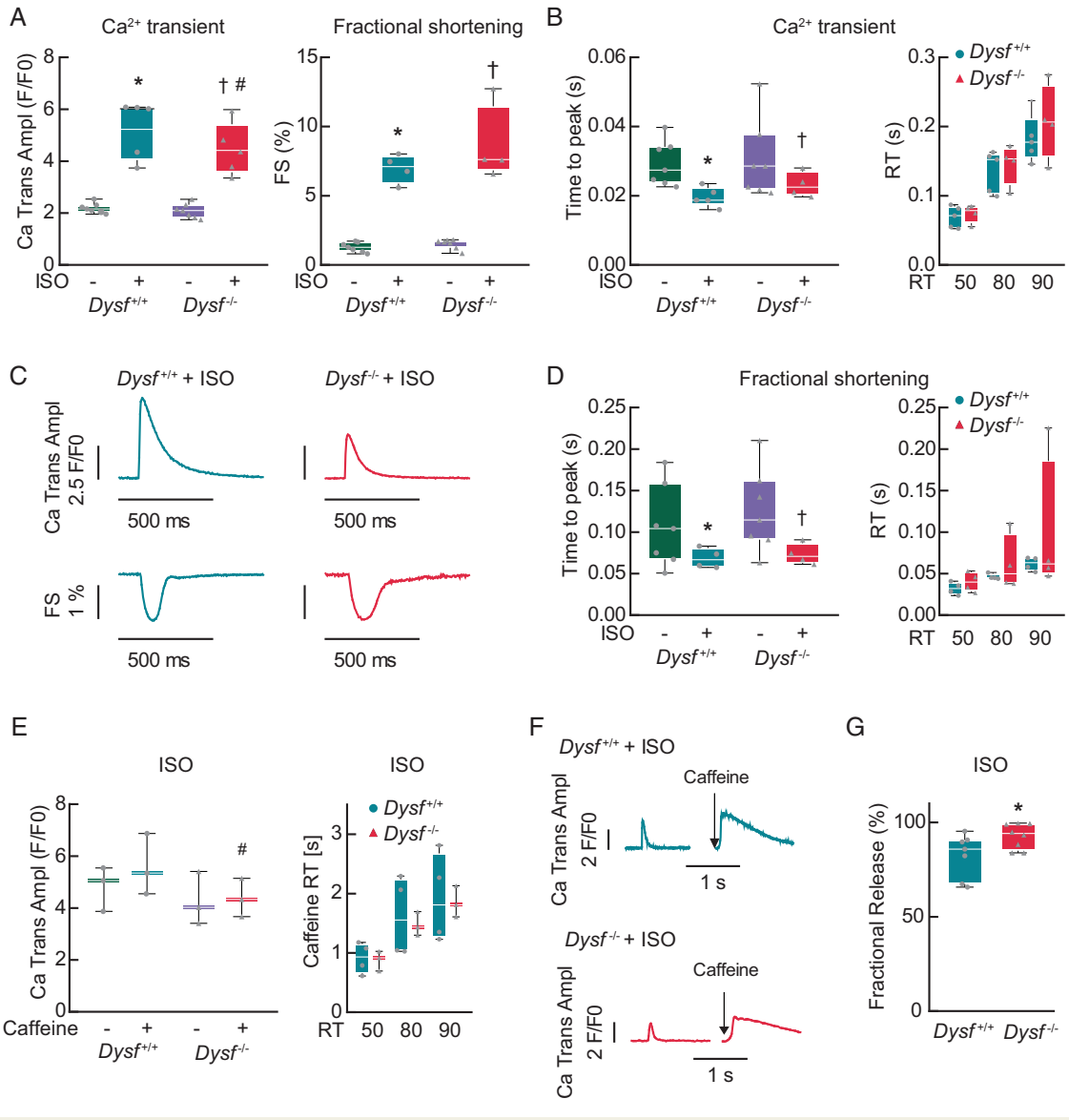

Figure 5 Ca^{2+} release phenotype under beta-adrenergic stress. (*A* and *B*) Ca^{2+} release of cardiomyocytes from male dysferlin-deficient ($Dysf^{-/-}$) mice is significantly decreased after induction of stress by isoprenaline (ISO). Isolated cardiomyocytes were loaded with fluo-4 and treated with the ß-AR agonist ISO (ISO, $c = 10^{-7}$ mol/L) in presence of 1 mmol/L Ca^{2+}. (*A*) CaT amplitudes (left) and fractional shortening (FS) (right) at 1 Hz. Mean ISO-induced CaT amplitude: $Dysf^{+/+}$ = 5.15 ± 0.31 F/F0, $Dysf^{-/-}$ = 4.35 ± 0.24 F/F0. (*B*) Time to peak and relaxation times (RT) of CaT amplitudes at 1 Hz. (*C*) Representative steady-state (1 Hz) CaT amplitudes and FS of wild-type ($Dysf^{+/+}$) and dysferlin-deficient cardiomyocytes. (*D*) Time to peak and RTs of FS at 1 Hz, $N = 7$ mice and ≥24 cells per group. (*E* and *F*) Decreased SR Ca^{2+} content in dysferlin-deficient cardiomyocytes after ISO. A 10 mol/L caffeine was applied to isolated ISO-treated cardiomyocytes. (*E*) Steady-state and caffeine-induced CaT amplitudes (mean: $Dysf^{+/+}$ = 5.58 ± 0.63 F/F0, $Dysf^{-/-}$ = 3.98 ± 0.31 F/F0) of ISO-treated cells and RTs of the caffeine-induced CaT of ISO-treated cells. (*F*) Representative steady-state (1 Hz) and caffeine-induced CaT amplitudes ISO-treated cells. (*G*) Fractional release (FR) of SR calcium content after ISO is significantly increased in dysferlin-deficient cardiomyocytes. Mean FR: $Dysf^{+/+}$= 83.33 ± 3.08%, $Dysf^{-/-}$ = 93.59 ± 2.06%, $N = 7$ mice and ≥11 cells per group. Nested *t*-test or nested ANOVA. $^{*}P \leq 0.05$ vs. $Dysf^{+/+}$, $^{\#}P \leq 0.05$ vs. $Dysf^{+/+}$+ISO, $^{\dagger}P \leq 0.05$ vs. $Dysf^{-/-}$. ANOVA, analysis of variance.

contributes to heart disease. In this study, we identify altered Ca^{2+} handling, especially under β-AR stimulation, in ventricular myocytes from dysferlin-deficient mice. We show that loss of dysferlin leads to a dramatic loss of transversal elements of the TATS (axialization) and that, owing to its role in TATS formation and maintenance, dysferlin is essential for excitation–contraction coupling.

In skeletal muscle, dysferlin is involved in formation of the T-tubule system, and in muscle development and regeneration.[4] In cardiac muscle, dysferlin plays a role in membrane repair,[9] but whether dysferlin is involved in TATS formation and development remained an open question. Dysferlin interacts with the LTCC and with caveolin-3 in the cardiomyocyte, supporting a model that involves a critical

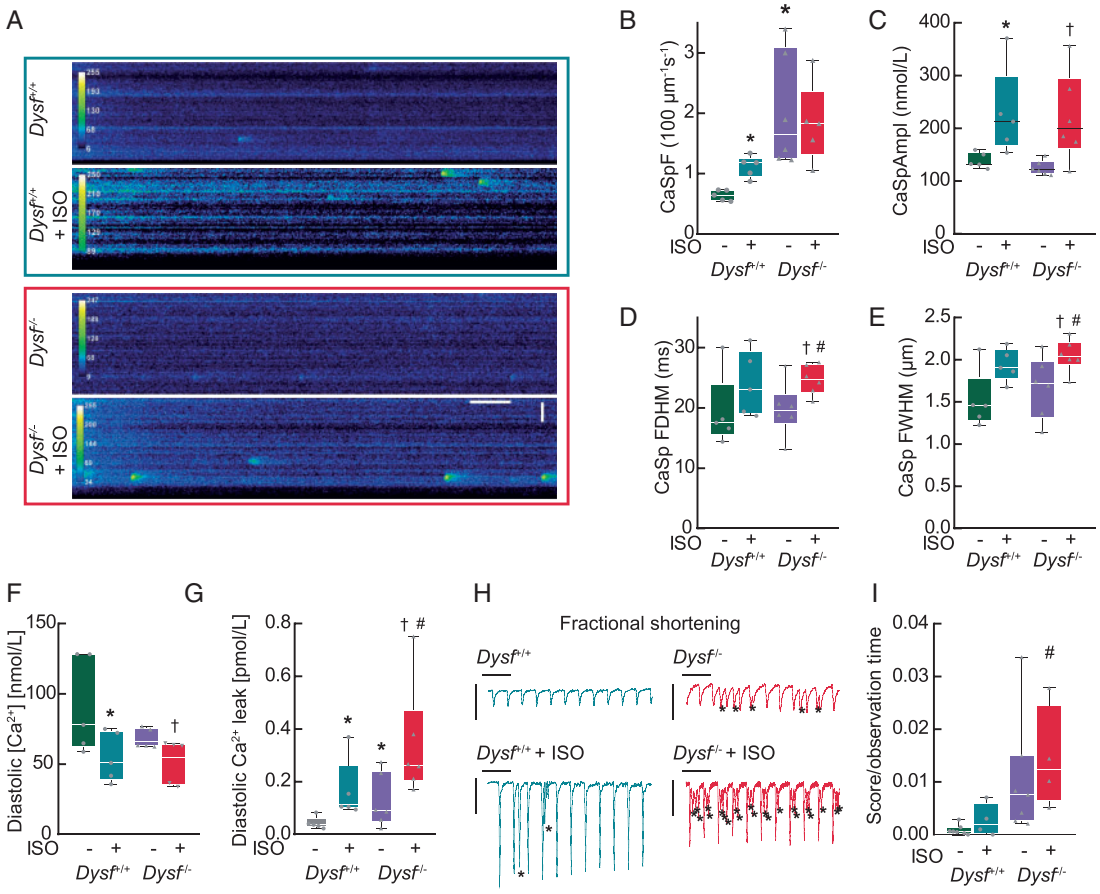

Figure 6 Ca^{2+} leak and pro-arrhythmia in dysferlin-deficient cardiomyocytes. (*A–G*) Ca^{2+} spark measurements reveal significantly increased SR Ca^{2+} leak in cardiomyocytes from male $Dysf^{-/-}$ mice. (*A*) Increased spark frequency of dysferlin-deficient ($Dysf^{-/-}$) cardiomyocytes leads to a significantly increased diastolic Ca^{2+} leak. Representative line scan images (ΔF/F0, 0.96 ms/line) of vehicle- and isoprenaline (ISO)-treated dysferlin-deficient and wild-type ($Dysf^{+/+}$) cardiomyocytes. Spark frequency (mean: $Dysf^{+/+}$= 0.65 ± 0.03 100 $\mu m^{-1}s^{-1}$, $Dysf^{-/-}$ = 1.88 ± 0.25 100 $um^{-1}s^{-1}$) (*B*), spatiotemporal properties of Ca^{2+} sparks, such as amplitude (*C*), full duration at half maximum (*D*) and spatial spread (full width at half maximum) (*E*), diastolic [Ca^{2+}] (*F*), and diastolic SR Ca^{2+} leak (*G*). Mean SR Ca^{2+} leak: $Dysf^{+/+}$ = 4.95 × 10^{-5} ± 9.40 × 10^{-6} nmol/L, $Dysf^{-/-}$ = 1.16 × 10^{-4} ± 2.50 × 10^{-5} nmol/L, $Dysf^{+/+}$ + ISO = 1.47 × 10^{-4} ± 2.27 × 10^{-5} nmol/L, $Dysf^{-/-}$ + ISO = 2.82 × 10^{-4} ± 4.05 × 10^{-5} nmol/L. Horizontal scale bar: 200 ms, vertical scale bar: 10 µm, $N \geq 4$ mice and ≥40 cells per group (nested ANOVA). (*H* and *I*). Pro-arrhythmogenic events in ISO-treated dysferlin-deficient cardiomyocytes (see *Figure 5*). (*H*) Original traces of fractional shortening after vehicle or ISO treatment (10^{-7} M) at 1 Hz showing spontaneous cellular arrhythmias (*). (*I*) Arrhythmia score per observation time. Mean: $Dysf^{+/+}$ = 9.31 × 10^{-4} ± 4.82 × 10^{-4}, $Dysf^{-/-}$ = 7.85 × 10^{-3} ± 4.04 × 10^{-3}, $Dysf^{+/+}$ + ISO= 2.67 × 10^{-3} ± 0.80 × 10^{-3}, $Dysf^{-/-}$ + ISO = 1.98 × 10^{-2} ± 0.70 × 10^{-2} (nested ANOVA), vertical scale bars: 0.05%, horizontal scale bars: 2 s. *$P \leq 0.05$ vs. $Dysf^{+/+}$, †$P \leq 0.05$ vs. $Dysf^{-/-}$ #$P \leq 0.05$ vs. $Dysf^{+/+}$ + ISO. ANOVA, analysis of variance.

function at the TATS, potentially similar to Bin1, a protein involved in skeletal muscle T-tubule biogenesis that recruits LTCC to the cardiac TATS and is involved in TATS morphogenesis. Our data show that dysferlin co-localizes with LTCC in the TATS. The appearance and formation of the tubular system correlates with dysferlin expression and its LTCC co-localization. Possibly, also the formation of LTCC-RyR2 couplons within these tubules correlates with dysferlin expression during postnatal development, hypothesizing a role of dysferlin in development and maintenance of the tubule network.

Changes in TATS structure detected here resemble the changes observed during development of HF including a global reorganization with loss of transversal elements. We did not find increased dysferlin expression in the pressure overload model. In contrast, the increased expression of dysferlin after MI indicates a compensatory and probably stabilizing role for dysferlin in membrane remodelling during HF development when membrane remodelling is remarkable.

Based on the structural and functional consequences of dysferlin loss that we identify here, we propose a model for the function of dysferlin and the pathophysiology of dysferlinopathy in the heart (*Figure 7*). Dysferlin is a tail-anchored protein that uses its C-terminal transmembrane domain as a membrane anchor in the TATS and in the plasma membrane. Dysferlin also possesses seven C2-domains that are potential Ca^{2+}-dependent membrane contact modules. When analysing the skeletal muscle function of dysferlin, we found evidence that dysferlin exerts the T-tubule morphogenic function by directly binding to the tubule membrane.[4] We here suggest that

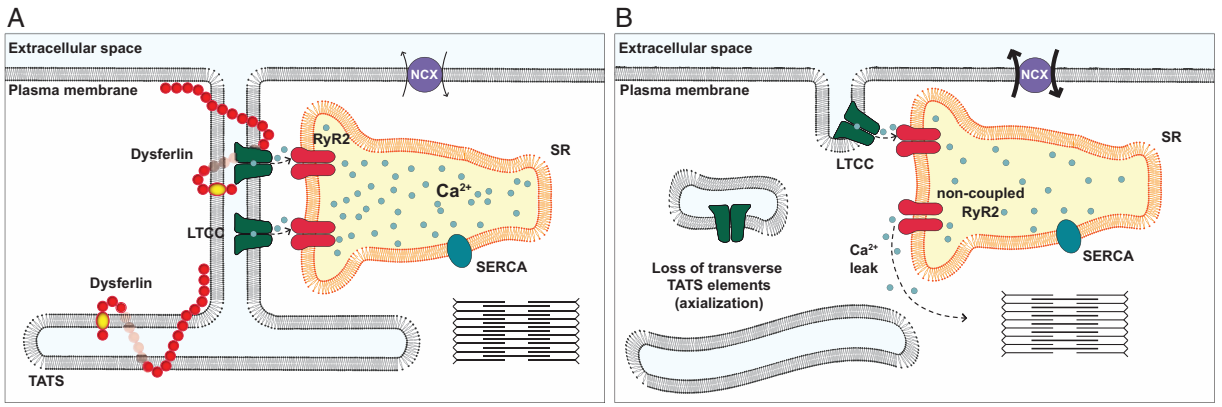

Figure 7 Model: dysferlin is essential for TATS structure and facilitates EC coupling in cardiomyocytes. (*A*) Dysferlin is C-terminally embedded in the plasma membrane and in the TATS membrane and structures intracellular membranes by additional binding through C2 domains. Dysferlin shapes and maintains the TATS structure in cardiomyocytes, supporting functional EC-coupling. (*B*) Upon dysferlin deficiency, TATS morphology is altered with loss of transversal elements (axialization). Consequently, LTCC and RyR2 loosen their association (non-coupled Ryr2, orphanization), leading to a Ca^{2+} leak, reduced SR Ca^{2+} content, and increased NCX activity. Dysregulated Ca^{2+} signalling triggers spontaneous Ca^{2+} sparks and primes the cardiomyocyte for pro-arrhythmic contractions. EC, excitation–contraction; SR, ; TATS, transverse-axial tubule system.

dysferlin binding by the cardiac TATS controls the ratio of transversal and axial TATS elements and that loss of dysferlin shifts this equilibrium by untightening the transversal element attachment to the plasma membrane and allowing its reorientation (*Figure* 7). This reorientation and remodelling of TATS structures likely results in disturbed microdomain Ca^{2+} signalling. Our model suggests that dysferlin interacts with LTCC and contributes to the maintenance of Ca^{2+}-handling. Although $I_{Ca,L}$ was reduced in dysferlin-deficient mice, the CaT, cell shortening and relaxation were not altered under basal conditions explaining the rather mild cardiac phenotype that is observed in dysferlin-deficient mice. In contrast, the amplification of CaT by β-AR stimulation with ISO and SR Ca^{2+} load were diminished in dysferlin-deficient myocytes. This is in agreement with studies showing that β-AR stimulation leads to significantly blunted inotropic and lusitropic responses in dysferlin-deficient hearts[9,12] highlighting the susceptibility of dysferlin-deficient hearts to stress.

We identified more frequent Ca^{2+} sparks in ventricular cardiomyocytes of dysferlin-deficient mice and consequently an even more pronounced SR Ca^{2+} leak under β-AR stimulation. Consistently, an increased number of pro-arrhythmic events was detected suggesting that a deficiency of dysferlin may increase the risk of arrhythmias. Reduced CaT after stress induction together with pro-arrhythmogenic events due to an SR Ca^{2+} leak suggest a primarily proarrhythmic phenotype that might be the cause of the decreased contractile function of the heart in dysferlinopathy.

Limitations

We would also like to reflect on the limitation of our study. (i) While generally the dysferlin-deficient mouse used in this study reliably models human disease with regard to the genetics (patients are often homozygous, or compound heterozygous) and the skeletal disease phenotype, species-specific differences between mouse and human may hamper the translation of these finding to human disease. (ii) Based on the CaT decay rate, we assume that SR Ca^{2+} buffering is largely unaffected in dysferlin deficiency. It would be desirable, however, to study caffeine-induced NCX current that was not measured in this study. (iii) The cardiomyocytes isolated from 1-year-old mice used in this study reflect the phenotype in dysferlinopathy patients with regard to late disease onset. However, the question if the cardiomyopathy found in older dysferlinopathy patients is causally linked to the genetic disease remains open. Also, it would be interesting to study progression of structural alteration during disease development in a time series experiment. (iv) We are suggesting that the TATS morphological changes in dysferlin-deficiency are indicative of a cellular pathology and correspond to alterations in Ca^{2+} handling that ultimately lead to arrhythmogenicity. It would be rewarding, therefore, to correlate MI and TAC TATS phenotype with dysferlin expression and dynamics and to study TATS morphology and Ca^{2+} changes concomitantly. (v) Our results and conclusions are based on experiments on isolated cardiomyocytes. Extrapolation of our findings on the *in vivo* situation in mice and also in humans remains challenging. Further studies will be required, in particular with regard to the predominantly pro-arrhythmic phenotype in dysferlin-deficient mice.

Conclusion

Taken together, dysferlin is essential for TATS structure and maintenance under normal and pathological conditions thereby facilitating proper excitation–contraction coupling and contraction. Loss of dysferlin leads to a massive structural reorganization with loss and axialization of TATS elements as well as abnormal Ca^{2+}-handling. The model proposed in this study could explain the structural role of dysferlin for the TATS as well as the functional consequences of dysferlin deficiency in the heart.

Supplementary material

Supplementary material is available at *Europace* online.

Acknowledgements

The authors thank Irmgard Cierny, Marc Ziegenbein, Tobias Goldak, Ines Müller, Timo Schulte, and Johanna Heine for technical assistance, the SFB 1002 service unit S01 (Disease Models) for TAC experiments and Eva Wagner for help with analysis of TATS orientation. The authors thank Anna Bulankina and Fleur Mason for comments on the manuscript.

Funding

This work was supported by grants from the Deutsche Forschungsgemeinschaft (DFG TH1538/1-1 and TH1538/3-1 to S.T., KL1868/5-1 to L.K., VO1568/3-1 and IRTG1816-TP12 to N.V.), and the Collaborate Research Council 'Modulatory units in heart failure' (SFB 1002/2, TP A10 to S.T., TP C07 to L.C.Z., TP A13 to N.V., TP D04 to K.T., and service project S01), by the Hunsmann foundation (to K.B.), by the VW Foundation (Project 131260/ZN2921 to S.T.), by the Else-Kröner-Fresenius Foundation (EKFS 2016_A20 to N.V., EKFS 2017_A137 to K.S.B.), and by the Horst and Eva-Luise Köhler Foundation (to S.T., J.H., K.B.). L.S.M. and S.W. are funded by the DFG SFB 1350 TP A6, by the ReForM C programme of the faculty, and the DZHK (Deutsches Zentrum für Herz-Kreislauf-Forschung; German Center for Cardiovascular Research). L.S.M. is funded by DFG (MA 1982/5-1 and 7-1), EU (SILICOFCM ID 777204). S.W. is funded by DFG grants WA 2539/4-1, 5-1, and 7-1.

Conflict of interest: none declared.

References

1. Bansal D, Campbell KP. Dysferlin and the plasma membrane repair in muscular dystrophy. *Trends Cell Biol* 2004;**14**:206–13.
2. Bulankina AV, Thoms S. Functions of vertebrate ferlins. *Cells* 2020;**9**:534.
3. Kerr JP, Ziman AP, Mueller AL, Muriel JM, Kleinhans-Welte E, Gumerson JD *et al.* Dysferlin stabilizes stress-induced Ca^{2+} signaling in the transverse tubule membrane. *Proc Natl Acad Sci USA* 2013;**110**:20831–6.
4. Hofhuis J, Bersch K, Büssenschütt R, Drzymalski M, Liebetanz D, Nikolaev VO *et al.* Dysferlin mediates membrane tubulation and links T-tubule biogenesis to muscular dystrophy. *J Cell Sci* 2017;**130**:841–52.
5. Nishikawa A, Mori-Yoshimura M, Segawa K, Hayashi YK, Takahashi T, Saito Y *et al.* Respiratory and cardiac function in Japanese patients with dysferlinopathy. *Muscle Nerve* 2016;**53**:394–401.
6. Wenzel K, Geier C, Qadri F, Hubner N, Schulz H, Erdmann B *et al.* Dysfunction of dysferlin-deficient hearts. *J Mol Med* 2007;**85**:1203–14.
7. Choi ER, Park S-J, Choe YH, Ryu DR, Chang S-A, Choi J-O *et al.* Early detection of cardiac involvement in Miyoshi myopathy: 2D strain echocardiography and late gadolinium enhancement cardiovascular magnetic resonance. *J Cardiovasc Magn Reson* 2010;**12**:31.
8. Rosales XQ, Moser SJ, Tran T, McCarthy B, Dunn N, Habib P *et al.* Cardiovascular magnetic resonance of cardiomyopathy in limb girdle muscular dystrophy 2B and 2I. *J Cardiovasc Magn Reson* 2011;**13**:39.
9. Han R, Bansal D, Miyake K, Muniz VP, Weiss RM, McNeil PL *et al.* Dysferlin-mediated membrane repair protects the heart from stress-induced left ventricular injury. *J Clin Invest* 2007;**117**:1805–13.
10. Tzeng H-P, Evans S, Gao F, Chambers K, Topkara VK, Sivasubramanian N *et al.* Dysferlin mediates the cytoprotective effects of TRAF2 following myocardial ischemia reperfusion injury. *J Am Heart Assoc* 2014;**3**:e000662.
11. Chase TH, Cox GA, Burzenski L, Foreman O, Shultz LD. Dysferlin deficiency and the development of cardiomyopathy in a mouse model of limb-girdle muscular dystrophy 2B. *Am J Pathol* 2009;**175**:2299–308.
12. Wei B, Wei H, Jin J-P. Dysferlin deficiency blunts β-adrenergic-dependent lusitropic function of mouse heart. *J Physiol* 2015;**593**:5127–44.
13. Lemckert FA, Bournazos A, Eckert DM, Kenzler M, Hawkes JM, Butler TL *et al.* Lack of MG53 in human heart precludes utility as a biomarker of myocardial injury or endogenous cardioprotective factor. *Cardiovasc Res* 2016;**110**:178–87.
14. Sperelakis N, Rubio R. An orderly lattice of axial tubules which interconnect adjacent transverse tubules in guinea-pig ventricular myocardium. *J Mol Cell Cardiol* 1971;**2**:211–20.
15. Forbes MS, Hawkey LA, Sperelakis N. The transverse-axial tubular system (tats) of mouse myocardium: its morphology in the developing and adult animal. *Am J Anat* 1984;**170**:143–62.
16. Cannell MB, Crossman DJ, Soeller C. Effect of changes in action potential spike configuration, junctional sarcoplasmic reticulum micro-architecture and altered t-tubule structure in human heart failure. *J Muscle Res Cell Motil* 2006;**27**:297–306.
17. Pieske B, Maier LS, Bers DM, Hasenfuss G. Ca^{2+} handling and sarcoplasmic reticulum Ca^{2+} content in isolated failing and nonfailing human myocardium. *Circ Res* 1999;**85**:38–46.
18. Heinzel FR, Bito V, Biesmans L, Wu M, Detre E, von WF *et al.* Remodeling of T-tubules and reduced synchrony of Ca^{2+} release in myocytes from chronically ischemic myocardium. *Circ Res* 2008;**102**:338–46.
19. Wei S, Guo A, Chen B, Kutschke W, Xie Y-P, Zimmerman K *et al.* T-tubule remodeling during transition from hypertrophy to heart failure. *Circ Res* 2010;**107**:520–31.
20. Seidel T, Navankasattusas S, Ahmad A, Diakos NA, Xu WD, Tristani-Firouzi M *et al.* Sheet-like remodeling of the transverse tubular system in human heart failure impairs excitation-contraction coupling and functional recovery by mechanical unloading. *Circulation* 2017;**135**:1632–45.
21. Bell RM, Mocanu MM, Yellon DM. Retrograde heart perfusion: the Langendorff technique of isolated heart perfusion. *J Mol Cell Cardiol* 2011;**50**:940–50.
22. Wagner E, Brandenburg S, Kohl T, Lehnart SE. Analysis of tubular membrane networks in cardiac myocytes from atria and ventricles. *J Vis Exp* 2014;**92**:e51823.
23. Cardoso-Moreira M, Halbert J, Valloton D, Velten B, Chen C, Shao Y *et al.* Gene expression across mammalian organ development. *Nature* 2019;**571**:505–9.
24. Bers D. *Excitation-Contraction Coupling and Cardiac Contractile Force*. 2nd ed. Netherlands: Springer; 2001.
25. Song L-S, Sobie EA, McCulle S, Lederer WJ, Balke CW, Cheng H. Orphaned ryanodine receptors in the failing heart. *Proc Natl Acad Sci USA* 2006;**103**:4305–10.